Bulletin of the National Research Centre

RESEARCH Open Access

# Elastic Properties of Cr-doped Mn Ferrite

M. H. Abdellatif and A. A. Azab*

## Abstract

**Background:** The mechanical properties of Mn-Cr ferrite of different compositions are important for industrial applications in everyday life. Ferrites are used in electric choke coils, electric transformers, and many other electronic and optical devices. The elastic properties can be understood by studying the longitudinal sound velocity ($V_l$) and shear velocity ($V_s$).

**Results:** The longitudinal sound velocity ($V_l$) and shear velocity ($V_s$) are measured at room temperature by pulse transmission technique at the frequency of 1659 Hz, which is ideally representing the mechanical properties of the ferrite crystal. The shear sound velocity was found to be around $4 \times 10^3$ m / s while the longitudinal sound velocity was ranging according to the doping concentration from $6 \times 10^3$ to $1 \times 10^4$ m / s. The behavior of Young's modulus ($E$), rigidity modulus ($n$), mean sound velocity ($V_m$), and Debye temperature ($\theta_D$) is quite similar, where a change in the slope was noticed at Cr concentration higher than 0.7 in the spinel lattice.

**Conclusion:** We have characterized the elastic properties of the spinel structure Mn-Cr ferrite with different Cr ion concentration at a fixed sound frequency using the pulse transmission technique. The longitudinal sound velocity showed an increase with increasing Cr ion concentration, the rigidity constant as well as Debye temperature, Isotropic compressibility, and the acoustic impedance showed behavioral change at Cr ion concentration x = 0.7 which is correlated to the intra-ionic distances change due to the replacement of Fe ions with smaller size Cr ions.

**Keywords:** Mn-Cr ferrite, Mechanical properties, Debye temperature, Acoustic impedance

## Introduction

Ferrites have been proven as important compounds that have a wide range of applications in the industry (Abdellatif et al., 2018; Abdellatif et al., 2017), research (Liakos et al., 2016; Abdellatif et al., 2015), physics (Abdellatif et al., 2018; Abdellatif et al., 2015; Abdellatif et al., 2012; Abdellatif et al., 2011), and chemistry of everyday life (Abdellatif et al., 2017; Abdellatif et al., 2016; Abdellatif et al., 2017; Abdellatif et al., 2018; Abdellatif & Azab, 2018). One of the important features of ferrites is its elastic properties; the importance of elastic properties arises due to the fact that studying mechanical and acoustic can give wide insight on the interatomic and interionic forces in solid and crystalline material (Modi et al., 2014; Patange et al., 2013; Modi et al., 2006). The study of elastic properties also helps one to calculate some thermodynamic coordinates such as the Debye temperature. Moreover, the variation of the elastic properties with gradually changing compositions is also important. Previous studies on Cu-Zn (Modi et al., 2006) and Ni-Zn (Rajesh Babu & Tatarchuk, 2018) show a linear variation of the elastic moduli with concentration. Young's modulus, the rigidity constant, the mean sound velocity, the transverse sound velocity, and the longitudinal sound velocity are known as the elastic parameters of solid crystals. Those parameters can be used to interpret the behavior of the crystalline solid on the basis of binding energy between atoms. Moreover, the Debye temperature can be calculated based on the mechanical parameters using the Anderson formula (Lakhani & Modi, 2010).

One more point, the elastic properties are important in the industry due to the direct relation to the strength of the material under various conditions. The ultrasonic pulse transmission technique is based on transmitting an acoustic pulse at one end of the solid and measuring the attenuation at the other end; accordingly, various mechanical parameters can be calculated. In this work, a systematic study of Mn-Cr ferrite of different compos-

* Correspondence: aliazab@hotmail.com
Solid State Physics Department, Physical Research Division, National Research Centre, El-Bohoos str., 12622, Dokki, Giza, Egypt

ition ($x$ = 0.2, 0.4, 0.7, 0.9, 1) is undertaken at room temperature. We have paid high attention to calculate the thermodynamical parameters and discuss their correlation with the ferrite structure, and the results are presented in this paper.

## Experimental details

Mn-Cr mixed ferrites of the chemical formula $MnCr_xFe_{2-x}O_4$ where $x$ = 0.2, 0.4, 0.7, 0.9, and 1 have been prepared by double sintering technique from high purity oxides. Namely, the oxides are manganese(II) oxide (MnO), iron(III) oxide ($Fe_2O_3$), and chromium(III) oxide ($Cr_2O_3$), all bought from Sigma-Aldrich. The oxides are mixed together in a stoichiometric ratio to obtain materials with general formula $MnCr_xFe_{2-x}O_4$. The mixed oxides were continuously grounded for 12 h in a ball miller model PM100 (Retsch, Germany). The oxide's powder was compressed into discs of 10 mm diameter and 3 mm thickness with the help of a home-made uniaxial press, by using an appropriate steel mold. The samples were pre-sintered at 800 °C for 8 h. Then, they were grinded to a fine powder and then pressed again into pellets of a rectangular form of 0.8 cm × 0.6 cm dimensions using a uniaxial press of pressure 3 × $10^5$ $N/m^2$, and the pellets are sintered at 1200 °C for 10 h with a heating rate of 4 deg/min. More details of this method are given in the earlier publication (Ahmed et al., 2012). The elastic properties have been measured by pulse transmission technique (Kohlhauser & Hellmich, 2013; Yu-Huai et al., 1985). In this method, a short pulse from a pulse generator is subjected to the sample through a copper rod using a PZT crystal (Piezoelectric Transducer), which is converted into the mechanical wave and on its arrival at the receiving point, and is converted back into an electrical signal, which is then amplified and fed to an oscilloscope. By knowing the dimensions of the sample and phase difference between the transmitted and received pulse, the sound velocity could be obtained. The sample is housed in a suitable sample holder made of copper rod. Calibration has been done to correct the delay of the sound wave at endpoints. The elastic parameter has been calculated using the following formulas (Venudhar & Mohan, 2002; Ravinder et al., 2001):

$$E = 2n(1 + \sigma) \tag{1}$$

where $n$ is the rigidity modulus calculated from $n = \rho V_s^2$ where $\rho$ is the density of the sample calculated by knowing the mass and dimensions of the sample, $V_s$is the sheer velocity, and $\sigma$ is the Poisson ratio.

$$\sigma = \frac{\left(V_\ell^2 - 2V_s^2\right)}{2\left(V_\ell^2 - V_s^2\right)} \tag{2}$$

Debye temperature $\theta_D$ as given by Anderson's formula (Venudhar & Mohan, 2002; Ravinder et al., 2001):

$$\theta_D = \left(\frac{V_m h}{k}\right)\left(\frac{3qN\rho}{4\pi M}\right)^{1/3} \tag{3}$$

$$V_m = 1/3\left(\frac{2}{V_s^3} + \frac{1}{V_\ell^3}\right)^{-1/3} \tag{4}$$

where $h$ is the Planck constant, $q$ is the number of atoms per molecule, $M$ is the molecular weight, and $V_m$ is the average sound velocity.

## Results

Figure 1 shows the shear and longitudinal sound velocity respectively as a function of Cr ion concentration at room temperature. It can be seen that the general trend is the increase of the sound velocity with increasing $Cr^{3+}$ ion concentration.

Figure 2 a and b show the rigidity and Young's modulus, respectively. It is clear from the figure that Young's modulus increases with increasing $Cr^{3+}$ ion concentration. The graph could be noted by two straight lines that intersect at $x$ = 0.7, which is the point at which the strain decreases by a value corresponding to the decrease in the mean free path of the oscillation.

Figure 3 shows the variation of one of the most important parameters of the thermodynamical coordinate, and it is the Debye temperature of the samples for all mixed ferrites versus average sound velocity. The figure shows that the Debye temperature varies linearly with the average sound velocity $V_m$. The Debye temperature $\theta_D$ has been calculated from the Anderson formula.

Figure 4 illustrates the isotropic compressibility of the sound wave and the acoustic impedance of the specimen for the sound wave. The figure shows that the concentration at $x$ = 0.7 has minimum isotropic compressibility and maximum acoustic impedance.

Figure 5 correlates the continuous decrease in the mean atomic weight with increasing $Cr^{3+}$ ion (51.996) concentration due to the fact that Cr ions replace Fe ions (55.847) in the spinel lattice, which is understood as a decrease in the inertia of the molecules of the spinel lattice in which it gets lighter due to ion Cr and Fe ion replacement.

Table 1 shows the variation of density ($\rho$) and longitudinal ($V_\lambda$), shear ($V_s$), and average sound velocity ($V_m$) with increasing $Cr^{3+}$ ion concentration; the trend of the acoustic and thermodynamical parameters can be followed in the table during the discussion.

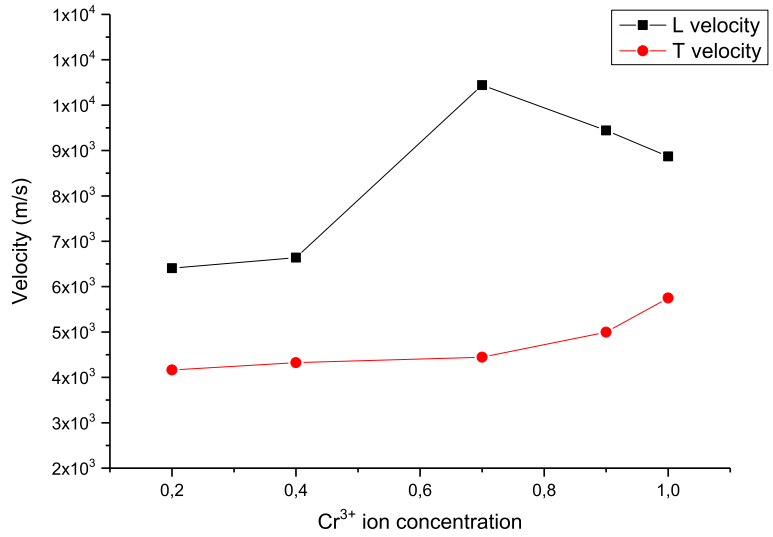


**Fig. 1** Variation of the shear and longitudinal sound velocity with $Cr^{3+}$ ion concentration in the spinel structure of Mn-Cr Ferrite

## Discussion

The mechanical properties of spinel ferrite can be fully understood by considering the interatomic distance of the spinel lattice. It is well known that the ionic radius of $Fe^{3+}$ (0.645 Å) is greater than $Cr^{3+}$ (0.615 Å) so that as the $Cr^{3+}$ content increases, the interionic distance decreases. As the bond strength increases Young's modulus, the rigidity modulus increases. In other words, one can understand from the experimental data that the binding between the ions of the investigated ferrite is increased successively with increasing $Cr^{3+}$ ion content (Mazen & Elmosalami, 2011; Bartůněk et al., 2018; Sattar & Rahman, 2003) which greatly affects the shear and longitudinal sound velocity in the ferrite slap as shown in Fig. 1. The figure shows an increase in the sound velocity with increasing $Cr^{3+}$ ion concentration. The longitudinal velocity shows a hump at $x$ = 0.7. The $Cr^{3+}$ ion is known to have a strong preference to the octahedral site, which replaces $Fe^{3+}$ content, refer to Table 1 for exact calculated values. We can fully understand the change of the sound velocity by studying its thermodynamical coordinates, since the response of the solid to the acoustic pulse depends on its interatomic arrangement, in a spinel structure, and there are two main interstitial sites, the octahedral (B) and tetrahedral site (A). The vibrating force constant then depends on the ion distribution in the crystal lattice; with the help of Waldron's method (Mazen & Abu-Elsaad, 2012), the force constant can be calculated using the following equations (Mazen & Abu-Elsaad, 2012):

$$K_t = 7.62 \times M_a \times \nu_1{}^2\, N/m \tag{5}$$

$$K_o = 10.62 \times M_b \times \nu_2{}^2\, N/m \tag{6}$$

where $\nu_1$ and $\nu_2$ are determined from the IR spectra, then $M_a$ and $M_b$ are the molecular weights of cations in sites A and B, respectively, according to the cation distribution predicted from X-ray. Moreover, the Debye temperature $\theta_d$ can be calculated using the following formula (Mazen & Abu-Elsaad, 2012):

$$\theta_D = \frac{hcV_{ab}}{k}, V_{ab} = \frac{V_a + V_b}{2} \tag{7}$$

where $V_{ab}$ is the average wave number of the absorption band in the FTIR spectrum, $h$ is the Planck constant, and $k$ is the Boltzmann constant.

The bulk modulus ($B$) of the solid is defined by as seen in Eq. 8 (Kittel, 2005):

$$B = \frac{1}{3}[C_{11} + 2C_{12}] \tag{8}$$

where $C_{11}$ and $C_{12}$ are the components of the elasticity tensor, for isotropic materials with cubic symmetry like spinel ferrites and garnets; $C_{11}$ is almost equal to $C_{12}$ that leads to $B = C_{11}$.

Hence, the force constant $k_{av} = aC_{11}$, where $k_{av}$ is the average force constant $K_{av} = \frac{(K_t + K_o)}{2}$.

The longitudinal elastic wave velocity and transverse wave velocity can be calculated from (Kittel, 2005):

$$V_l = (C_{11}/\Delta x)^{1/2}, V_t = V_l/\sqrt{3} \tag{9}$$

However, the mean elastic wave velocity is defined by:

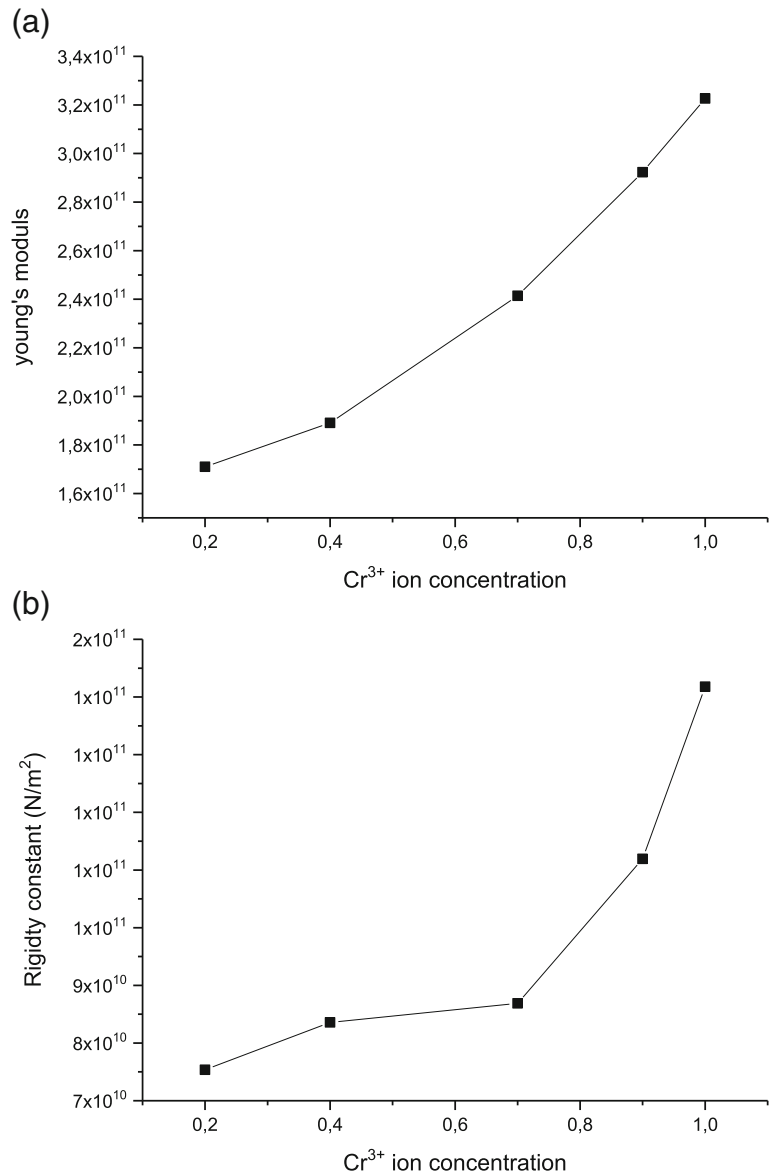


**Fig. 2** **a** Variation of Young's modulus with varying $Cr^{3+}$ ion concentration. **b** Rigidity constant with varying $Cr^{3+}$ ion concentration

$$V_m = \frac{1}{3}\left[\frac{2}{V_l^2} + \frac{1}{V_t^2}\right]^{-1/3} \tag{10}$$

Rigidity modulus $G$ is defined by (Raj et al., 2004):

$$G = \Delta x \cdot V_t^2 \tag{11}$$

Poisson's ratio is defined by:

$$P = 3B - \frac{2G}{6B} + 2G \tag{12}$$

In that sense Young's modulus will be defined as:

$$E = \frac{1}{\frac{P}{2G}} \tag{13}$$

Then by using Anderson's formula, the Debye temperature can be calculated using the following equation (Raj et al., 2004):

$$\theta_d = \frac{h}{K}[3N_a/4\pi V_{atomic}]^{1/3} V/m \tag{14}$$

where $V_{atomic}$ is the mean atomic volume, $V_{atomic} = (M/\Delta x)/q$, $M$ is the molecular weight, $N_a$ is Avogadro's number, and $q$ is the number of atoms in the formula unit. However, the importance of elastic properties in spinel structure

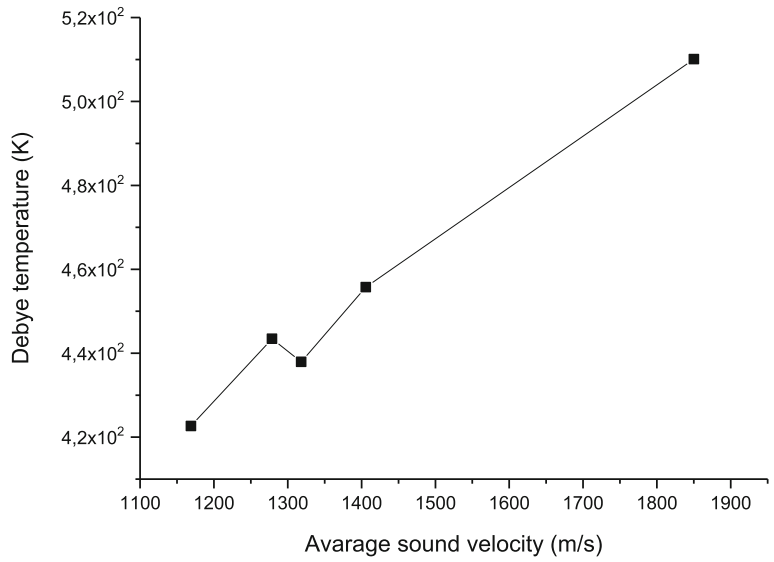


**Fig. 3** Variation of the Debye temperature with varying average sound velocity

and all isotropic crystals is the possibility to that it can define the behavior of the binding energies in the crystal lattice. In general, the relation between the average sound velocity increases linearly with the Debye temperature, which is the relation between acoustic parameters defined by sound velocities in the material and the thermodynamic parameters defined by the Debye temperature. However, since ferrite materials are mostly porous which can affect the measured parameters, the velocity should be corrected to zero porosity using the Mackenzie formula (Showry & Murthy, 1991). The hardness of the material can be determined by the Poisson ratio. It is found that material with a low value of Poisson ratio less than 0.25 is brittle, and those with high value are ductile.

The change in the binding energy due to replacement of Fe by Cr ions also has its effect on the rigidity and Young's modulus shown in Fig. 2; however, a change in the slope can be noticed at $x = 0.7$. This can be understood as the point at which the strain decreases by a value that corresponds to the decrease in the mean free path of the oscillation. The same trend was obtained, where the rigidity modulus increases slightly up to $x = 0.7$, after which it increases suddenly up to $x = 1$. That can be understood as the interionic space changes with changing ion concentration that has a critical value at

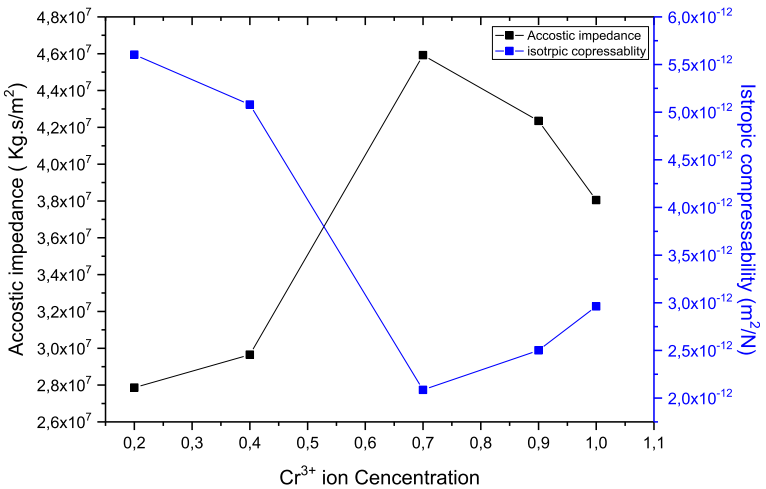


**Fig. 4** Variation of the isotropic compressibility and acoustic impedance with varying $Cr^{3+}$ ion concentration in Mn-Cr spinel ferrite

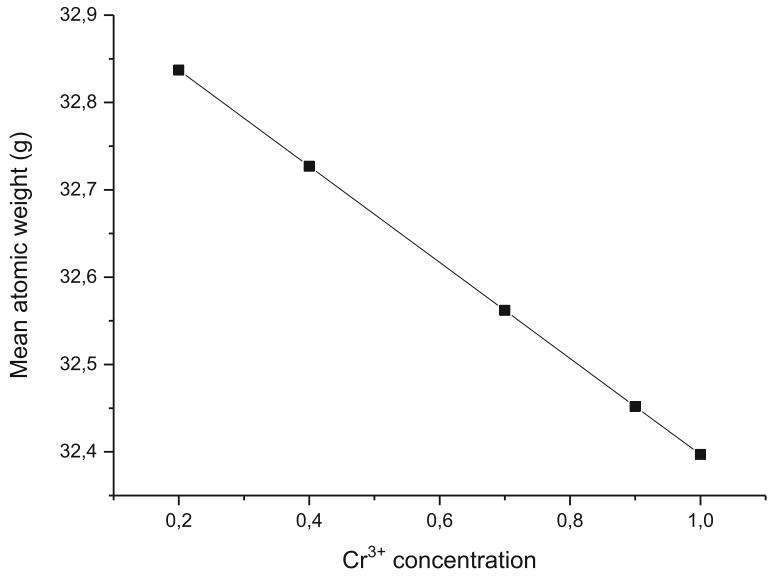


**Fig. 5** Variation of the mean atomic value with varying $Cr^{3+}$ ion concentration

$x$ = 0.7. The data in Fig. 1 enhances our expectation where a hump is obtained at $x$ = 0.7. The highest normal mode of vibration for the crystal can be found considering the Debye temperature which is shown in Fig. 3. The Debye temperature defines the thermodynamical coordinates of all mixed ferrites versus average sound velocity. It is found that in our samples, the Debye temperature varies linearly with the average sound velocity $V_m$. The Debye temperature $\theta_D$ has been calculated from the Anderson formula. The linear increase of the Debye temperature corresponds to the linear increase of the normal vibrational mode of the crystal, which is correlated to the interatomic distances due to the replacement of Fe ions by Cr ions in the spinel lattice.

The controlling principles of ultrasonic are associated with material properties such as density and modulus of elasticity. In general, there are two types of ultrasonic waves based on material, the bulk waves and guided waves. The bulk waves propagate inside the material while the guided wave propagates near the surface or along with the interface. The longitudinal waves are those with the displacement in the same direction as travel direction while shear waves are based on the displacement of the amplitude in a direction perpendicular to the propagation direction. According to a theoretical model of attenuation, ultrasonic waves in polycrystalline materials are mainly attenuated by scattering at structure boundaries, grains, grain boundaries, and inclusions. The number of scattering is proportional to the grain volume while the attenuation is a function of the grain size and frequency of the wave. The attenuation coefficient $\alpha$ is a sum of the individual coefficient for scattering and absorption over all frequencies (Mazen & Elmosalami, 2011; Bartůněk et al., 2018; Sattar & Rahman, 2003; Muralidhar et al., 1992; Srinivas Rao et al., 2002; Ravinder & Reddy, 2003).

The attenuation coefficient can be defined as the logarithmic decrement between two consecutive pulse echoes (Lakhani & Modi, 2010; Yu-Huai et al., 1985):

$$\alpha\left(\frac{\mathrm{dB}}{\mathrm{mm}}\right) = 20 \log \frac{\left(\frac{S_1}{S_2}\right)}{2d}, \tag{15}$$

Where $S_1$ and $S_2$ are the amplitude of two consecutive back wall echoes, and $d$ is the thickness of the specimen in millimeter. It follows that the velocity of the ultrasound waves in polycrystalline or bulk materials is primarily controlled by elastic modulus and density which is directly related to its microstructure.

**Table 1** Variation of density ($\rho$), longitudinal ($V_l$), shear ($V_s$), and average sound velocity ($V_m$) with increasing $Cr^{3+}$ ion concentration

| Concentration ($x$) of Cr ion | $V_l$(m/s) | $V_s$(m/s) | $V_m$ (m/s) | $\rho$ (kg/m$^3$) |
|---|---|---|---|---|
| 0.2 | 6405.768 | 4162.62 | 1168.985 | 4349.018 |
| 0.4 | 6639.212 | 4325.87 | 1318.206 | 4466.313 |
| 0.7 | 10441.945 | 4444.73 | 1278.671 | 4397.435 |
| 0.9 | 9441.012 | 4995.42 | 1405.765 | 4485.510 |
| 1 | 8871.003 | 5748.98 | 1850.092 | 4289.476 |

The isotropic compressibility changes accordingly, as shown in Fig. 4. The figure shows that the concentration at $x$ = 0.7 has a minimum isotropic compressibility and maximum acoustic impedance. The isotropic compressibility is related to the density and longitudinal velocity by the formula $K_s = \frac{1}{\rho V_\ell}$, and the acoustic impedance of the sound energy is calculated from $Z = \rho V_\lambda$. The isotropic compressibility can be understood by looking at the change in the mean atomic weight due to ion replacement shown in Fig. 5. The continuous decrease in the mean atomic weight with increasing $Cr^{3+}$ ion is due to the difference in ionic weight of $Cr^{3+}$ (51.996) instead of iron (55.847). The variation of the bulk modulus and the average sound velocity with Cr ion concentration is shown in the Appendix, and the two graphs show a behavioral change at $x$ = 0.7 in accordance with previous data. In general, a microstructure that strains the lattice or interrupts its continuity reduces the elastic modulus and the velocity of ultrasonic waves. Ferrite materials are made of grain and grain boundaries, and hence, its response to acoustic pulse depends on its microstructure performance. Considering the magnetic nature of ferrite, then magnetocrystalline anisotropy comes into play. The magnetocrystalline anisotropy is a measure for the magnetic energy resistance to the movement of the domain walls, while the domain walls are free to move at a temperature where the magnetic anisotropy is equal to zero. That means the substance undergoes a maximum strain for given stress, or in other words, the longitudinal and shear sound velocity show a decrease with increasing temperature. In the case of an externally applied magnetic field that saturates the sample, the longitudinal and shear sound velocity are slightly higher than the demagnetized state. However, in a mono-domain state, the sound velocities decrease constantly with the increase in temperature (Mazen & Elmosalami, 2011; Bartůněk et al., 2018; Sattar & Rahman, 2003; Muralidhar et al., 1992; Srinivas Rao et al., 2002; Ravinder & Reddy, 2003).

## Conclusion

We have characterized the elastic properties of the spinel structure Mn-Cr ferrite with different Cr ion concentration at a fixed sound frequency using the pulse transmission technique. The longitudinal sound velocity showed an increase with increasing Cr ion concentration; the rigidity constant as well as the Debye temperature, the isotropic compressibility, and the acoustic impedance showed behavioral change at Cr ion concentration $x$ = 0.7 which is correlated to the intra-ionic distance change due to the replacement of Fe ions with smaller size Cr ions.

## Appendix

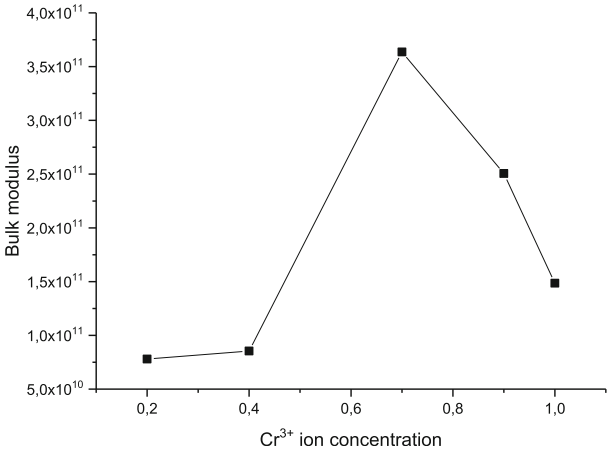


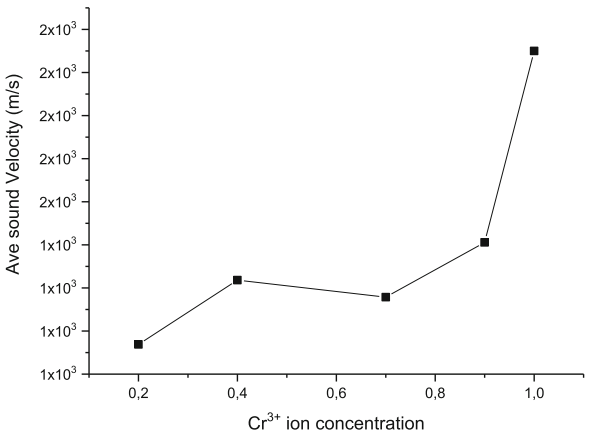


**Acknowledgements**
The author is very grateful to the Solid State Department, National Research Centre, for their valuable help provided.

**Authors' contributions**
The authors read and approved the final manuscript.

**Funding**
The research was financed by the authors.

**Availability of data and materials**
Not applicable

**Ethics approval and consent to participate**
Not applicable

**Consent for publication**
Not applicable.

**Competing interests**
The authors declare that they have no competing interests.

Received: 11 February 2019 Accepted: 11 June 2019
Published online: 15 July 2019

## References

Abdellatif MH, Abdelrasoul GN, Scarpellini A, Marras S, Diaspro A (2015) Induced growth of dendrite gold nanostructure by controlling self-assembly aggregation dynamics. J Colloid Interface Sci 458. https://doi.org/10.1016/j.jcis.2015.07.055

Abdellatif MH, Azab AA (2018) Fractal growth of ferrite nanoparticles prepared by citrate-gel auto-combustion method. Silicon. https://doi.org/10.1007/s12633-017-9711-1

Abdellatif MH, Azab AA, Salerno M (2018) Effect of rare earth doping on the vibrational spectra of spinel Mn-Cr ferrite. Mater Res Bull 97:260–264. https://doi.org/10.1016/j.materresbull.2017.09.012

Abdellatif MH, El-Komy GM, Azab AA, Salerno M (2018) Crystal field distortion of $La^{3+}$ ion-doped Mn-Cr ferrite. J Magn Magn Mater 447. https://doi.org/10.1016/j.jmmm.2017.09.040

Abdellatif MH, Ghosh S, Liakos I, Scarpellini A, Marras S, Diaspro A, Salerno M (2016) Effect of nanoscale size and medium on metal work function in oleylamine-capped gold nanocrystals. J Phys Chem Solid 89. https://doi.org/10.1016/j.jpcs.2015.09.012

Abdellatif MH, Song JD, Choi WJ, Cho NK (2012) In/Ga inter-diffusion in InAs quantum dot in InGaAs/GaAs asymmetric quantum well. J Nanosci Nanotechnol 12. https://doi.org/10.1166/jnn.2012.6280

Abdellatif MH, Song JD, Choi WJ, Cho NK, Lee JI (2011) Quantum dot-like effect in InGaAs/GaAs quantum well. EPJ Appl Phys 55. https://doi.org/10.1051/epjap/2011100342

Abdellatif MHH, Azab AAA, Moustafa AMM (2017) Dielectric spectroscopy of localized electrical charges in ferrite thin film. J Electron Mater:1–7. https://doi.org/10.1007/s11664-017-5782-4

Abdellatif MHH, El-Komy GMM, Azab AAA, Moustafa AMM (2017) Oscillator strength and dispersive energy of dipoles in ferrite thin film. Mater Res Express 4:076410. https://doi.org/10.1088/2053-1591/aa7e57

Ahmed MAA, Afify HHH, El Zawawia IKK, Azab AAA (2012) Novel structural and magnetic properties of Mg doped copper nanoferrites prepared by conventional and wet methods. J Magn Magn Mater 324:2199–2204. https://www.sciencedirect.com/science/article/abs/pii/S0304885312001229. Accessed 25 Aug 2018.

Bartůněk V, Sedmidubský D, Huber Š, Švecová M, Ulbrich P, Jankovský O (2018) Synthesis and properties of nanosized stoichiometric cobalt ferrite spinel. Mater (Basel, Switzerland) 11. https://doi.org/10.3390/ma11071241

Kittel C (2005) Introduction to solid state physics. Wiley, USA. https://www.amazon.de/Introduction-Solid-Physics-Charles-Kittel/dp/047141526X/ref=asc_df_047141526X/?tag=googshopde-21&linkCode=df0&hvadid=310619680508&hvpos=1o1&hvnetw=g&hvrand=13600327134509980065&hvpone=&hvptwo=&hvqmt=&hvdev=c&hvdvcmdl=&hvlocint=&hvlocphy=9043440&hvtargid=pla-454232548305&psc=1&th=1&psc=1&tag=&ref=&adgrpid=60989744559&hvpone=&hvptwo=&hvadid=310619680508&hvpos=1o1&hvnetw=g&hvrand=13600327134509980065&hvqmt=&hvdev=c&hvdvcmdl=&hvlocint=&hvlocphy=9043440&hvtargid=pla-454232548305.

Kohlhauser C, Hellmich C (2013) Ultrasonic contact pulse transmission for elastic wave velocity and stiffness determination: influence of specimen geometry and porosity. Eng Struct 47:115–133. https://doi.org/10.1016/J.ENGSTRUCT.2012.10.027

Lakhani VK, Modi KB (2010) Al3+-modified elastic properties of copper ferrite. Solid State Sci 12:2134–2143. https://doi.org/10.1016/J.SOLIDSTATESCIENCES.2010.09.012

Liakos IL, Abdellatif MH, Innocenti C, Scarpellini A, Carzino R, Brunetti V, Marras S, Brescia R, Drago F, Pompa P (2016) Antimicrobial lemongrass essential oil-copper ferrite cellulose acetate nanocapsules. Molecules. 21. https://doi.org/10.3390/molecules21040520

Mazen SA, Abu-Elsaad NI (2012) IR spectra, elastic and dielectric properties of Li–Mn ferrite. ISRN Condens Matter Phys 2012:1–9. https://doi.org/10.5402/2012/907257

Mazen SA, Elmosalami TA (2011) Structural and elastic properties of Li-Ni ferrite. ISRN Condens Matter Phys 2011:1–9. https://doi.org/10.5402/2011/820726

Modi KB, Shah SJ, Pathak TK, Vasoya NH, Lakhani VK, Yahya AK (2014) Improvement in elastic properties of CuAl0.4Fe1.6O4 spinel ferrite by rapid thermal cooling. In: AIP Conf. Proc. Am Inst Phys, pp 1115–1117. https://doi.org/10.1063/1.4872872.

Modi KB, Trivedi UN, Sharma PU, Lakhani VK, Chhantbar MC, Joshi HH (2006) Study of elastic properties of fine particle copper-zinc ferrites through infrared spectroscopy

Muralidhar M, Nanda Kishore K, Ramana YV, Hari Babu V (1992) Elastic and plastic behavior of lead and silver doped BiSrCaCuO superconductors. Mater Sci Eng B 13:215–219. https://doi.org/10.1016/0921-5107(92)90166-7

Patange SM, Shirsath SE, Jadhav SP, Hogade VS, Kamble SR, Jadhav KM (2013) Elastic properties of nanocrystalline aluminum substituted nickel ferrites prepared by co-precipitation method. J Mol Struct 1038:40–44. https://doi.org/10.1016/J.MOLSTRUC.2012.12.053

Raj B, Rajendran V, Palanichamy P (2004) Science and technology of ultrasonics, Alpha Science International.

Rajesh Babu B, Tatarchuk T (2018) Elastic properties and antistructural modeling for nickel-zinc ferrite-aluminates. Mater Chem Phys 207:534–541. https://doi.org/10.1016/J.MATCHEMPHYS.2017.12.084

Ravinder D, Balachander L, Venudhar Y (2001) Elastic behaviour of manganese substituted lithium ferrites. Mater Lett 49:205–208. https://doi.org/10.1016/S0167-577X(00)00369-4

Ravinder D, Reddy PVB (2003) Composition of room temperature elastic properties of mixed Li–Cu ferrites. Mater Lett 57:4575–4577. https://doi.org/10.1016/S0167-577X(03)00165-4

Sattar AA, Rahman SA (2003) Dielectric properties of rare earth substituted Cu-Zn ferrites. Phys Stat Sol 200:415–422. https://doi.org/10.1002/pssa.200306663

Showry K, Ramana Murthy S (1991) Elastic behaviour of Mn-Zn and Mg-Zn ferrites. https://onlinelibrary.wiley.com/doi/pdf/10.1002/crat.2170260322. Accessed 8 Jan 2019.

Srinivas Rao S, Chandra Shekhar Reddy A, Ravinder D, Ravinder Reddy B, Linga Reddy D (2002) Ultrasonic investigation on mixed manganese–zinc ferrite. Mater Lett 56:175–177. https://doi.org/10.1016/S0167-577X(02)00435-4

Venudhar Y, Mohan KS (2002) Elastic behaviour of lithium–cobalt mixed ferrites. Mater Lett 55:196–199. https://doi.org/10.1016/S0167-577X(01)00645-0

Yu-Huai S, Huang H-J, Fu-Sheng L (1985) Ultrasonic pulse transmission/echo technique for sound velocity measurements in high temperature and high pressure liquid metals. Jpn J Appl Phys 24:79. https://iopscience.iop.org/article/10.7567/JJAPS.24S1.79/pdf. Accessed 8 Jan 2019.

## Publisher's Note